J Mater Sci (2016) 51:2079–2089
DOI 10.1007/s10853-015-9518-7

Enhancement of gas–solid photocatalytic activity of nanocrystalline TiO_2 by SiO_2 opal photonic crystal

Ping Li[1,2] · Yuan Wang[1] · Sheng-Li Chen[1] · Ai-Jun Wang[1]

Received: 23 August 2015 / Accepted: 18 October 2015 / Published online: 5 November 2015

Abstract A series of nc-TiO_2/SiO_2 opal composite photocatalytic membranes were fabricated through coating a nanocrystal TiO_2 (nc-TiO_2) layer onto a SiO_2 opal photonic crystal layer and used as catalysts for photodegradation of gaseous acetaldehyde under 380 nm monochromatic light and white light irradiation. The photonic band gap (PBG) of the SiO_2 photonic crystal was designed at the vicinity of the electronic band gap of TiO_2 and tuned by the size of SiO_2 microspheres constructing the SiO_2 opals. It was found that the nc-TiO_2/SiO_2 opal composite membrane, with the PBG of the SiO_2 photonic crystal overlapping with the absorption edge of TiO_2, exhibited the highest photocatalytic activity, which was 1.5 times that of a control photocatalytic membrane—the membrane of nc-TiO_2 coated on a disordered porous SiO_2 film. The farther the photonic PBG is away from the absorption edge of TiO_2, the lower the photocatalytic activity of the composite membranes; when the nc-TiO_2/SiO_2 opal composite membrane catalyst with PBG was completely outside of the absorption edge of TiO_2, the photocatalytic enhancement was not found. The photocatalytic enhancement is attributed to the enhanced light harvest of TiO_2 resulting from the absorption of reflected light at PBG of photonic crystal and attributed to the light localization of photonic crystal inside the nc-TiO_2.

✉ Sheng-Li Chen
slchen@cup.edu.cn

[1] State Key Laboratory of Heavy Oil Processing and Department of Chemical Engineering, China University of Petroleum, Changping, Beijing 102249, China

[2] Key Laboratory for Green Chemical Process of Ministry of Education and Wuhan Institute of Technology, Hongshan 430073, Wuhan, China

Introduction

As the optical response of TiO_2 is limited in ultraviolet light with wavelength shorter than 387 nm, considerable efforts have been made to enhance the light harvest of TiO_2, therefore to increase the production of the photogenerated carriers and improve the photoactivity of TiO_2 [1]. The available methods for enhancing the light harvest of TiO_2 can be classified into two routes. The first is to expand the TiO_2 ultraviolet light absorption to visible light, such as dye sensitization [2], quantum dots sensitization [3], metal ion doping [4], nonmetal doping [5], and narrow band gap semiconductor coupling [6]. The second is to intensify the interaction of light with the photocatalyst, such as enhancing multiple light scattering by large particles or spherical voids [7], utilizing surface plasmon resonance of noble metal nanoparticles incorporated in TiO_2 [8].

In recent years, a new method for enhancing the photocatalytic activity of TiO_2 through the introduction of photonic crystals (PCs) has attracted a great deal of attention since Ozin research group [9] firstly reported the amplification of the photo-oxidation of methylene blue on nanocrystalline TiO_2 (nc-TiO_2) inverse opal PCs. When the red edge of the photonic band gap (PBG) is designed at the absorption edge of TiO_2, the decay rate of methylene blue on nc-TiO_2 inverse opal PCs is two times that on plain nc-TiO_2. The role of the inverse opal is to offer high specific surface area [10] and increase the path length of light through the slow photon effect at the edge of the PBG [11, 12]. Afterwards, the efforts of coupling inverse opal with other techniques [13, 14], like incorporation of plasmonic nanoparticles [15, 16], quantum dots sensitization [3, 17, 18], doping of nonmetal [19] and metal [20, 21], and modification with conducting polymers [22, 23], have been

made to synergistically improve the photocatalytic performance of TiO_2. However, when the PBG of inverse opal coincided with the absorption edge of TiO_2, the photoactivity of nc-TiO_2 would be suppressed due to the high reflectivity at this region [9]. That is, the single layer of inverse opal cannot use the reflected light at the EBG of the TiO_2. Mihi and Míguez constructed a dye-sensitized solar cell with bilayer structure [24–26] by spin-coating nc-TiO_2 film on the top of TiO_2 inverse opal PCs to enhance light harvest. The enhancement of light harvest was attributed to the dielectric mirror effect and the corresponding photon localization effect at the PBG of PCs. In order to use both the photon localization effect and the light reflection of PCs at the PBG, instead of structuring the photoactive material such as TiO_2 into inverse opal, our research group created bilayer photocatalysts through coupling nc-TiO_2 with SnO_2 inverse opal film [27, 28], and investigated their photocatalytic activity through the degradation of methylene blue in water solution (liquid–solid catalytic reaction) and Rhodamine B deposited on the TiO_2 (solid–solid catalytic reaction). The photocatalytic activity of the composite membranes was enhanced remarkably compared to that of TiO_2 film when the PBG of SnO_2 inverse opal was optimized to overlap with the electric band gap (EBG) of TiO_2, and even higher than that of TiO_2 inverse opal membrane. However, the study cannot distinguish the enhancement by the light-harvesting effect from that by the chemical doping effect. Besides, the preparation process of SnO_2 inverse opal is complicated and its quality is poorly repeatable.

In this work, we fabricated nc-TiO_2/SiO_2 opal composite membranes through coupling TiO_2 with SiO_2 opal PCs. Because the fabrication of SiO_2 opal PCs is much more easy and more duplicable than that of TiO_2 and SnO_2 inverse opal PCs, and because the SiO_2 is photochemically inert and transparent in the EBG of TiO_2, the nc-TiO_2/SiO_2 opal composite membrane is ideal material for us to investigate the effect of PCs on the catalytic activity of nc-TiO_2. The process to fabricate nc-TiO_2/SiO_2 opal composite membrane is shown in Scheme 1. Different from the previous study using the degradation of dye in liquid state or solid state as the probe reaction, in this work, gaseous degradation of acetaldehyde was used as probe reaction. The photoactivity of nc-TiO_2/SiO_2 opal with different PBGs was compared to that of a nc-TiO_2 film deposited on a disordered SiO_2 film and that of a conventional nc-TiO_2 film. The highest rate constant was obtained for nc-TiO_2 coupled to SiO_2 opal with the PBG overlapping with the absorption edge of TiO_2.

Experimental

Materials

Tetraethoxysilane (98 %, Acros) and Ludox AS-40 silica gel (Du Pont) were used to prepare silica monospheres. Tetraethoxysilane was freshly distilled before use. The Ludox AS-40 silica gel had a SiO_2 content of 41.8 wt%, SiO_2 average diameter of 31.62 nm, and relative standard deviation in diameter of 7.5 %. Titanium (IV) isopropoxide (98+%, Acros) was used to prepare nanocrystalline titania. Other chemicals of analytical grade were purchased from the Beijing Chemical Factory (China) and used without further purification, and double-distilled water was used in all the experiments. Glass slides (75 × 25 × 1 mm) were cleaved into two pieces along the long sides and used as substrates. All the glass slides were soaked in a Piranha solution overnight for hydrophilic treatment. The Piranha solution contained 30 mL of 40 wt% hydrogen peroxide and 70 mL of 98 wt% sulfuric acid. After that, the substrates were rinsed three times with water and ethanol, respectively, and finally dried in air.

Preparation of SiO_2 opal film

SiO_2 opal PCs with different PBGs were used in this work. The PBG of PCs was tuned by the size of the monodispersed SiO_2 microspheres assembled to the PCs. The preparation procedure is described as follows.

First, monodispersed SiO_2 microspheres were synthesized by seed-growth method using Ludox AS-40 silica gel as seeds [29]. In detail, a methanol solution containing

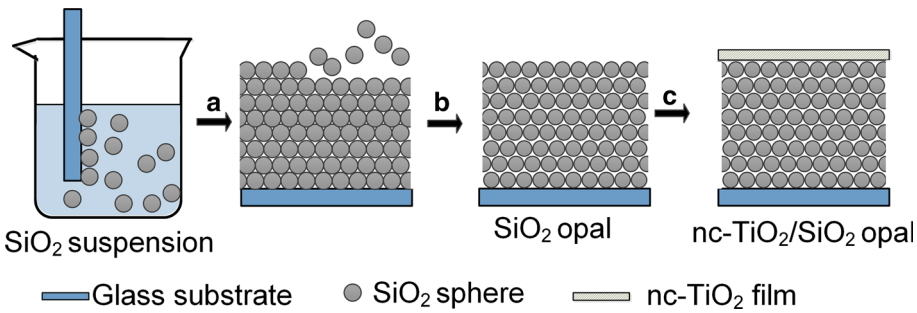

Scheme 1 Preparation steps of nc-TiO_2/SiO_2 opal composite membrane: *a* self-assembly of SiO_2 spheres on glass substrate; *b* calcination of SiO_2 opal film at 450 °C, 2 h; *c* spin-coating nc-TiO_2 film on SiO_2 opal and then calcination of the obtained composite membrane at 450 °C for 2 h

tetraethoxysilane and another methanol solution containing ammonium hydroxide and water were added dropwise into a methanol solution containing seeds, water, and ammonia at 35 °C under 200 rpm of stirring condition. When the SiO_2 seeds grew to desired size, stop dropping, and concentrate the monodisperse SiO_2 microspheres through centrifugation. Five monodispersed SiO_2 microspheres were prepared, and their sizes were measured to be 151, 170, 189, 198, and 214 nm by dynamic light scattering (DLS) on a Malvern Zetasizer Nano Series.

Then, SiO_2 opal PCs were fabricated via the room temperature floating self-assembly (RTFSA) technique developed by our research group [30, 31]. Monodispersed SiO_2 microspheres were dispersed into the mixture of ethanol and water (3:1 in volume ratio) to a concentration of 30 wt%. A glass substrate was dipped into the silica suspension, then quickly withdrawn from the suspension, and afterwards put horizontally on the experiment table. A PCs film with highly ordered hexagonal close-packing was obtained on the glass substrate when the solution was evaporated completely. By this technique, a SiO_2 opal PCs film with several square centimeters can be fabricated rapidly within 10 min. Finally, the glass slide with SiO_2 opal film on it was calcined at 450 °C for 2 h in air. The preparation of SiO_2 opal film is easy and duplicable, and the intensity of the reflectance peak of all the SiO_2 opal PCs fabricated in our work held at 30–40 %, confirming the high reproducibility of the SiO_2 opal.

A disordered SiO_2 film was used as the control sample, which was prepared from suspension of polydispersed SiO_2 microspheres by the RTFSA technique as that for the SiO_2 opal film. Polydispersed SiO_2 microspheres are the mixture of monodispersed SiO_2 microspheres with diameters of 151, 170, 189, 198, and 214 nm.

Preparation of nc-TiO_2/SiO_2 opal composite membranes

Nanocrystalline TiO_2 (nc-TiO_2) was synthesized via hydrothermal method [32]. Acetic acid (6 g) was added dropwise into 29.3 g of titanium isopropoxide under stirring condition at room temperature, and then stirred for 15 min, the mixture was added dropwise into 150 mL of water and then sonicated for half an hour. Thereafter, the suspension was peptized with 2.4 mL of 65 % nitric acid at 78 °C and stirred for 75 min and then autoclaved at 220 °C for 12 h. To form films, the resultant sol was concentrated by evaporation of water in vacuum at 30 °C until the TiO_2 content of the suspension reached to 10 wt%. Finally, polyethylene glycol 2000 (10 wt% by weight of the nc-TiO_2) was added to the suspension followed by stirring overnight.

The obtained suspension was spin-coated on the SiO_2 opal film with the spin rate of 2000 rpm. After dried at room temperature and calcined at 450 °C for 2 h, a nc-TiO_2/SiO_2 opal composite membrane was obtained. For comparison, nc-TiO_2/SiO_2-dis composite membrane was fabricated by spin-coating the nc-TiO_2 layer onto a disordered SiO_2 film using the same process. The thickness of nc-TiO_2 film was controlled to ~500 nm.

Structural and optical characterization of membranes

Optical properties of the prepared membrane samples were evaluated by measuring their transmission spectra and reflectance spectra using an UV–Vis spectrometer (Sp-1702, Shanghai Spectrum Instrument Co. Ltd., China). Scanning electron microscopy (SEM) was used to determine the morphology of the multilayer film. The top views and cross sections were obtained with a field-emission SEM (FEI Quanta 200F) operating at 20 kV. A thin layer of gold was sputtered onto the samples prior to SEM imaging. High-resolution transmission electron microscopy (HRTEM) images were obtained on a JEM-2100 LaB6 microscope (JEOL, Japanese) operating at 200 kV. Samples for TEM measurements were dispersed in ethanol, dropped on a carbon-coated microgrid.

Photocatalytic performance test

The photocatalytic performance of the as-prepared composite membranes was tested by the photodegradation of gaseous acetaldehyde under white light or monochromatic light irradiation (see Scheme 2). The white light of 2 mW cm^{-2} was obtained from a 150 W Xe lamp (Zolix LHX150). The monochromatic light at 380 nm with a light intensity of 1.2 mW cm^{-2} was obtained by placing a

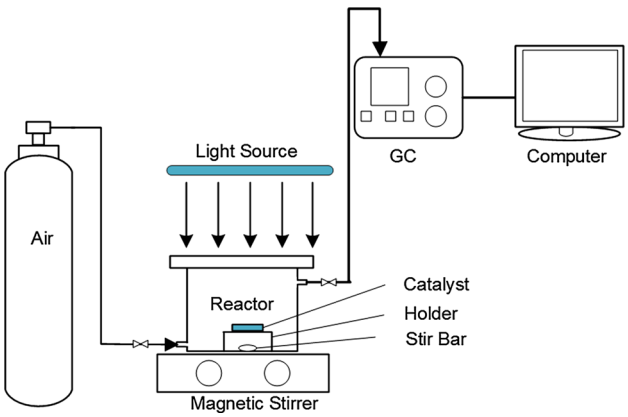

Scheme 2 The schematic diagram of the photocatalytic performance test

380 nm filter in front of a 500 W Xe lamp (Zolix LSH-X500). A composite membrane on a sample holder and a stir bar were placed into an airtight reactor of 872 mL. The area of all the membranes used herein was 5 cm^2. After blowing the reactor with dry air for 10 min, 5 μL of 8 wt% acetaldehyde aqueous solution was injected into the reactor under stirring. After the complete evaporation of the acetaldehyde solution, the gas was stirred in dark for 120 min to reach adsorption–desorption equilibrium. Then, 1 mL of gas was withdrawn every 15 min and analyzed by the gas chromatography (GC) equipped with FID detector and a HP-PLOT Q column. When the gas concentration remained unchanged, the lamp was switched on, and 1 mL gas was withdrawn every 30 min and analyzed by GC. The photodegradation of acetaldehyde follows the first-order decay rate law, and the kinetic rate constant was obtained from the logarithmic plot of the relative concentration ($\ln(C_t/C_0)$), as a function of time t, where C_0 is the initial concentration of acetaldehyde and C_t is the concentration of acetaldehyde at time t. To investigate the reproducibility of the photocatalytic activity test, we repeated the photocatalytic activity test on an nc-TiO_2 membrane three times, and the results demonstrated the high reproducibility of the photocatalytic activity test.

Results and discussions

Figure 1 shows the top view and cross section images of nc-TiO_2 film characterized by SEM. The surface morphology of nc-TiO_2 film has uniform porous structure with a disordered arrangement of homogeneous nanocrystalline particles. Bare films were transparent and colorless in the natural light. The cross section of SEM image showed that a 470-nm-thick nc-TiO_2 layer was formed by spin-coating. The TEM image of the prepared nc-TiO_2 particles showed that the nanocrystalline size was 10–20 nm (see Fig. 2a). The HRTEM image shown in Fig. 2b displayed the crystalline interplanar spacing of the nc-TiO_2 particles which was about 0.352 nm, corresponding to the (101) planes of anatase TiO_2 [33].

The absorbance spectrum of nc-TiO_2 film coated on glass substrate was measured, as shown in Fig. 3. The band gap energy of nc-TiO_2 is determined by Tauc formula applying the direct band gap energy:

$$(\alpha h\nu)^2 = K\left(h\nu - E_g\right), \tag{1}$$

where α is the absorption coefficient, $h\nu$ is the photon energy, K is a constant, and E_g is the band gap energy [11]. The dependence of $(\alpha h\nu)^2$ on $h\nu$ is shown in the inset of Fig. 3. The band gap energy was calculated from the extrapolated value (the dash lines to the x axis) of $h\nu$ at $\alpha = 0$ [11, 34]. The nc-TiO_2 film showed the band gap energy of 3.26 eV (corresponding to the wavelength of 380 nm), indicating the anatase phase of the TiO_2.

For evaluation of the role of PBG in photocatalytic performance, five SiO_2 opal PCs were fabricated from different sizes of silica spheres according to modified Braggs law [35]:

$$\lambda = 2\sqrt{\frac{2}{3}}D\sqrt{n_{SiO_2}^2 f + n_{air}^2(1-f) - \sin^2\theta}, \tag{2}$$

where λ is the wavelength of the PBG, D is the size of SiO_2 sphere, n_{SiO_2} and n_{air} are the refractive index of SiO_2 and air respectively, f is the fill factor of SiO_2 phase, which is generally taken as 0.74, and θ is the incident angle of light, $\theta = 0$ for normal incidence.

The PBGs of the fabricated SiO_2 opal PCs were estimated to be at the edge of, overlapped with, and out of the absorption edge of TiO_2, respectively. The average diameters of the prepared SiO_2 spheres were 151, 170, 189, 198, and 214 nm.

Previous study showed that the higher enhancement of photocatalytic activity could be achieved by the PCs with

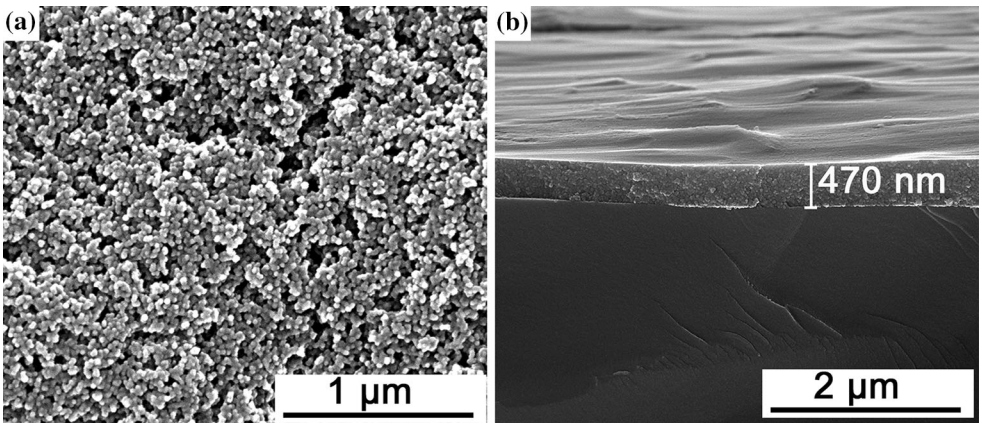

Fig. 1 SEM images of top view (**a**) and cross section (**b**) of nc-TiO_2 film

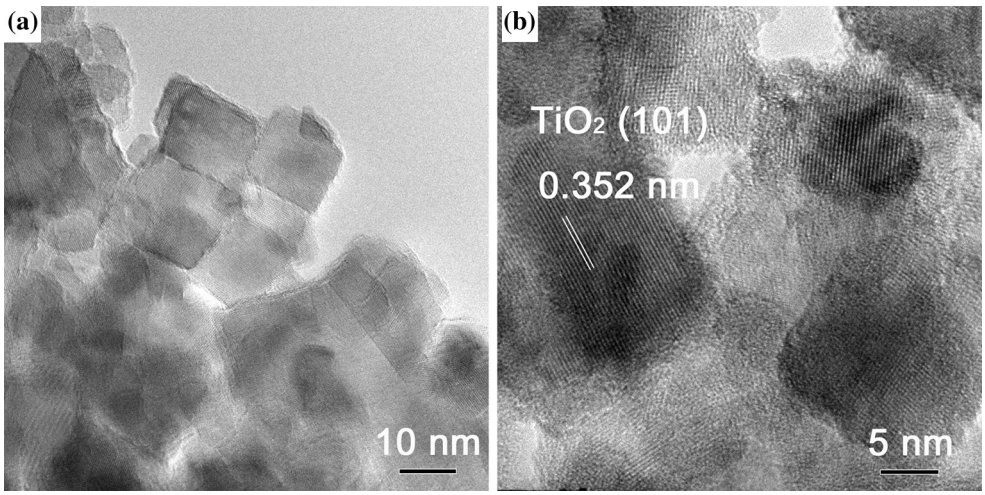

Fig. 2 TEM images of the synthesized nc-TiO_2 particle

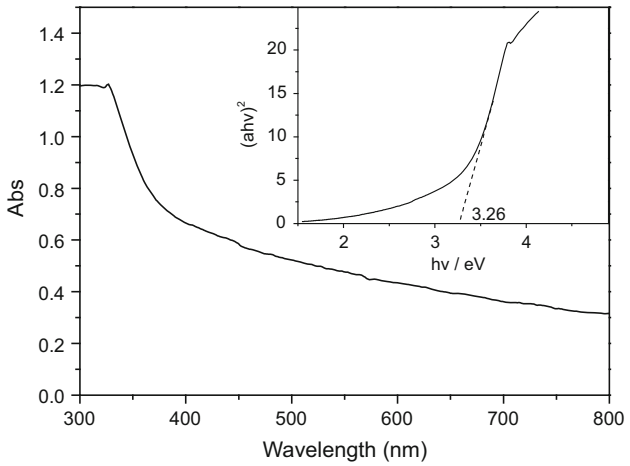

Fig. 3 The UV–Vis absorption spectrum of nc-TiO_2 film. The *inset* is the dependence of $(\alpha hv)^2$ on hv for the calculation of the band gap energy for the nc-TiO_2

higher degree of order [36]. Therefore, it is essential to prepare PCs with high quality. The SEM images of SiO_2 opal, as shown in Fig. 4, demonstrate that the PCs had high degree of order and a face-centered cubic (fcc) arrangement of SiO_2 spheres with the close-packed plane (111) parallel to the substrate. The inset in Fig. 4a displays the photographs of the corresponding SiO_2 opal PCs, which shows that the PCs were uniform and the area of the PCs could extend to several square centimeters.

Scanning electron micrographs of the cross sections of the as-prepared nc-TiO_2/SiO_2 opal composite membranes are displayed in Fig. 5. Likewise, the SiO_2 spheres were arranged orderly in all the nc-TiO_2/SiO_2 opal composite membranes, whereas it was found that the SiO_2 spheres were arranged randomly in the disordered SiO_2 layer (Fig. 5f). In addition, the thickness of nc-TiO_2 film for all the samples was controlled to 500 ± 30 nm (Fig. 5), by adjusting the spin-coating speed and the concentration of the spin-coating suspension. Hence, the effect of nc-TiO_2 thickness on photocatalytic performance [37] can be avoided.

The reflectance spectra of the PCs assembled from different sizes of SiO_2 monospheres are shown in Fig. 6. It can be seen that the PCs samples made of silica microspheres of 151, 170, 189, 198, and 214 nm had pronounced PBGs, and these PBGs were centered at 333, 350, 380, 400, and 458 nm, respectively, demonstrating high quality of these samples. The corresponding PCs film is denoted as SiO_2 opal-x, where x refers to the PBG position of the PCs.

The absorption edge of anatase TiO_2 is represented by the shaded area as shown in Fig. 6. Thus, according to their PBGs, the prepared PCs are classified into four types: (1) having PBG overlapping with the absorption edge of nc-TiO_2, represented by SiO_2 opal-380; (2) having PBG coinciding with the absorption red edge of nc-TiO_2, represented by SiO_2 opal-400; (3) having PBG coinciding with the absorption blue edge of nc-TiO_2, represented by SiO_2 opal-350; and (4) having PBG far away from the absorption edge of nc-TiO_2, represented by SiO_2 opal-333 and SiO_2 opal-458.

Photocatalytic degradation of acetaldehyde gas at room temperature was used as the probe reaction to evaluate the photocatalytic performance of nc-TiO_2/SiO_2 opal PCs composite membranes. Figure 7 shows a logarithmic plot of the relative concentration of acetaldehyde as a linear function of irradiation time for nc-TiO_2/SiO_2 opal composite membrane and nc-TiO_2/SiO_2-dis composite membrane, confirming the first-order photodegradation of acetaldehyde. The experiment for study of photocatalytic activity was performed under the white light from a 150 W Xe lamp. Disordered SiO_2 film (SiO_2-dis) was used as the

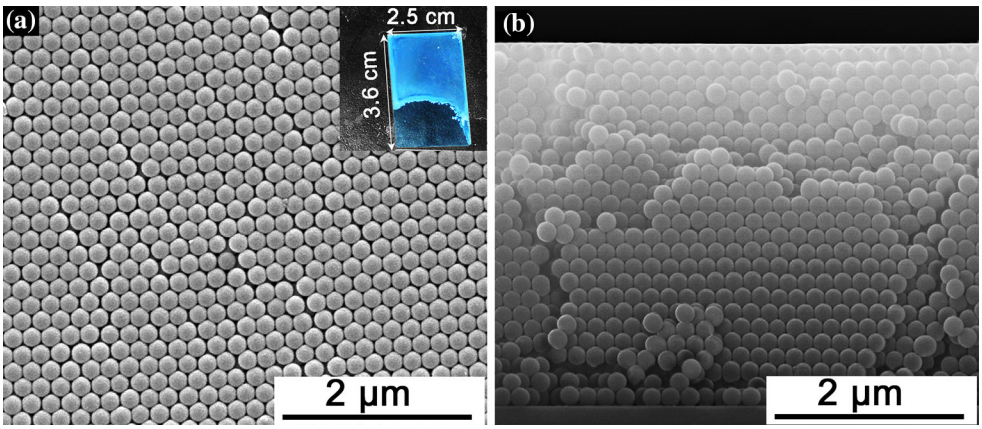

Fig. 4 SEM images of the top view (**a**) and the cross section (**b**) of the same piece of SiO_2 opal. The SiO_2 opal was grown from 198 nm SiO_2 microspheres suspension. The *inset* in **a** shows the photograph of the SiO_2 opal under natural light illumination (Color figure online)

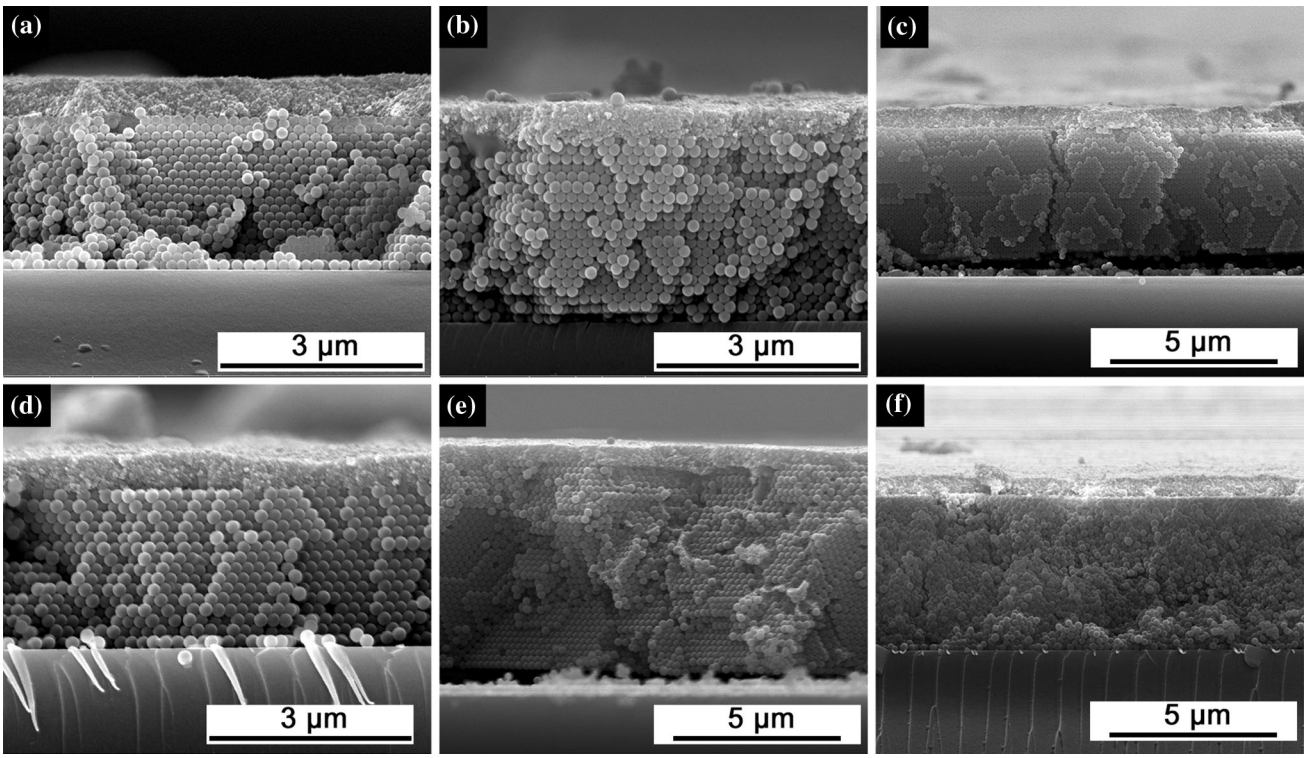

Fig. 5 SEM images of cross sections of nc-TiO_2/SiO_2 opal composite membrane (**a**–**e**) and nc-TiO_2/SiO_2-dis composite membrane (**f**). The sphere sizes in samples **a**–**e** are 151, 170, 189, 198, and 214 nm, respectively

blank, which showed almost no degradation of acetaldehyde under irradiation. The photocatalytic activity of nc-TiO_2/SiO_2-dis increased by 19 % compared to that of the plain nc-TiO_2 film on a glass substrate. As shown in Figs. 1 and 5, the thickness of nc-TiO_2 film on glass substrate was controlled to the exact same as that on SiO_2-dis and on SiO_2 opal films to eliminate the effect of TiO_2-thickness on photocatalytic performance. In addition, as shown in Fig. 6, the disordered SiO_2 film had no PBG in the reflectance spectrum and was inert in photocatalytic activity. Therefore, the photocatalytic enhancement of nc-TiO_2/SiO_2-dis compared to nc-TiO_2 film (see Fig. 7) was attributed to the diffuse scattering of the discorded SiO_2 film. Previous study has also confirmed that the light scattering alone can enhance the photovoltaic performance of a dye-sensitized solar cell up to 25 % [7]. Therefore, the strong diffuse scattering effect of the disordered SiO_2 in PCs could not be ignored, so that the nc-TiO_2/SiO_2-dis

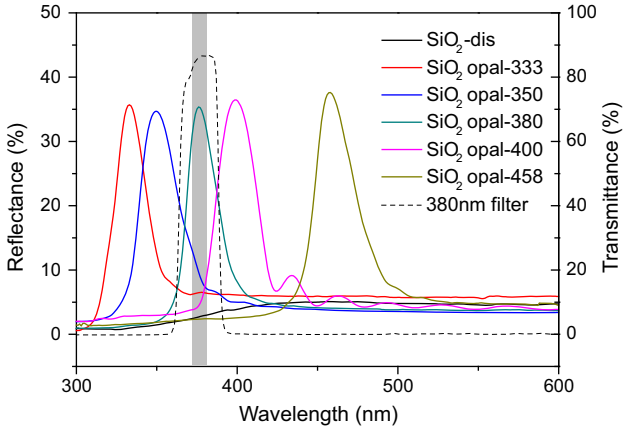

Fig. 6 The UV–Vis reflectance spectra of SiO_2 opal with different PBGs. The *dashed line* represents the transmission spectrum of the band-pass filter of 380 nm. The *shaded area* indicates the absorption edge of the TiO_2 (Color figure online)

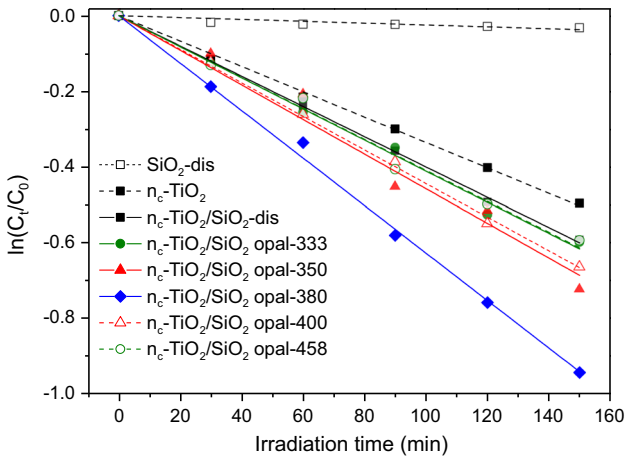

Fig. 7 The first-order photodegradation of acetaldehyde under white light irradiation of 2.0 mW cm^{-2}. The reaction conditions were as follows: room temperature, 5 cm^{-2} of the photocatalyst film in 872 mL reactor filled with air of 25 % relative water humidity and 200 ppmv gaseous acetaldehyde (Color figure online)

composite membrane was used as the control catalyst in this work. The kinetic constants of acetaldehyde degradation over nc-TiO_2/SiO_2 opal and nc-TiO_2/SiO_2-dis, as listed in Table 1, were calculated from the slope of the linear relationship between the logarithmic relative concentration and the irradiation time.

To compare the photocatalytic performance quantitatively, the enhancement factor (EF) was calculated as the ratio of the decay rate constant of nc-TiO_2/SiO_2 opal to that of nc-TiO_2/SiO_2-dis. The EF of nc-TiO_2/SiO_2 opal with various PBG is shown in Fig. 8.

Figure 8 shows that the maximum EF of 1.57 was achieved for nc-TiO_2/SiO_2-380 opal, which attributed to the dielectric mirror effect and the photon localization

Table 1 Kinetic constants and regression coefficients (R^2) of acetaldehyde degradation under white light irradiation of 2.0 mW cm^{-2}

Sample	Kinetic constant ($\times 10^{-3}$ min^{-1})	R^2
nc-TiO_2/SiO_2-dis	4.00	0.999
nc-TiO_2/SiO_2 opal-333	4.11	0.992
nc-TiO_2/SiO_2 opal-350	4.30	0.992
nc-TiO_2/SiO_2 opal-380	6.28	0.995
nc-TiO_2/SiO_2 opal-400	4.44	0.998
nc-TiO_2/SiO_2 opal-458	4.09	0.989

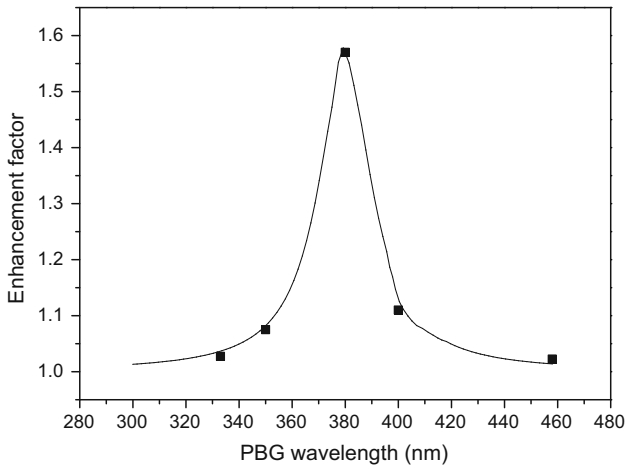

Fig. 8 Enhancement factor for nc-TiO_2/SiO_2 opals with PBGs under white light irradiation in comparison with the control of nc-TiO_2/SiO_2-dis

effect of the PCs. When light strikes the nc-TiO_2/SiO_2 opal-380 composite membrane, the light with wavelength shorter than 380 nm is completely absorbed by nc-TiO_2 film, therefore producing oxidizing holes and reducing electrons, whereas the light with wavelength longer than 380 nm passes through the nc-TiO_2 with hardly absorption. For the light with wavelength coinciding with the absorption edge of anatase at 380 nm, a small portion of the light is absorbed by nc-TiO_2 film, while another portion of the light penetrates nc-TiO_2 film and is reflected by the SiO_2 opal-380 PCs. On the one hand, the reflected light can be absorbed again by nc-TiO_2 film [27, 28], hence improving the light harvest of nc-TiO_2 film. On the other hand, optical interference takes place when the light being transmitted and reflected, and these resonant photons are partially localized in the nc-TiO_2 film [24, 38], thus improving the light–matter interaction, and the light absorption of TiO_2. As a consequence of the two effects, more electron–hole pairs were photogenerated, and a remarkable enhancement of photocatalytic performance was achieved for nc-TiO_2 coupled to SiO_2 opal-380 PCs.

A slight increase of photoactivity with the EF of 1.08–1.11 is found when the PBG of SiO_2 opal PCs partially overlaps with the absorption edge of TiO_2, as is the case of nc-TiO_2/SiO_2 opal-350 and nc-TiO_2/SiO_2 opal-400. In previous studies [13, 23, 39], the slow photon effect in TiO_2 at the edge of the PBG can increase the path length of light and then enhance the light absorption of TiO_2 when the PBG edge of the TiO_2 inverse opal is designed at the absorption edge of TiO_2. In our work, the PBG edge of SiO_2 opal-350 and SiO_2 opal-400 is designed at the absorption edge of TiO_2. For the nc-TiO_2/SiO_2 opal-350 composite membranes, the slow photons effect at blue edge of the PBG has no effect on light absorption of TiO_2 owing to the completely absorption during its first pass through TiO_2. However, the slow photons effect at red edges of the PBG is effective owing to the partial absorption during its first pass through TiO_2, and the remaining light was reflected by SiO_2 opal-350 and it propagated with strongly reduced group velocity during its second pass through TiO_2. Thus, the path length of light in TiO_2 increased and then the light absorption of TiO_2 enhanced. Likewise, for the nc-TiO_2/SiO_2 opal-400, the slow photons effect at blue edge is effective to enhance the absorption of TiO_2. Nevertheless, the slow photons effect at red edge has no effect owing to hardly any absorption of the reflected light through TiO_2 at this wavelength of light. However, as the intensity of the reflection at 380 nm, which is at the red edge of PBG of SiO_2 opal-350 or the blue edge of PBG of SiO_2 opal-400, is far weaker than that of SiO_2 opal-380, the enhancement factor of nc-TiO_2/SiO_2 opal-350 and nc-TiO_2/SiO_2 opal-400 is much less than nc-TiO_2/SiO_2 opal-380. The EFs of nc-TiO_2/SiO_2 opal-333 and nc-TiO_2/SiO_2 opal-458 were found to be negligible. The PBG of this type of PCs is completely out of the absorption edge of anatase. In the case of nc-TiO_2/SiO_2 opal-333, the light at the PCs' PBG would be completely absorbed by nc-TiO_2 film before it got to the SiO_2 opal-333, so the reflection effect at PBG was eliminated due to the high absorption. For nc-TiO_2/SiO_2 opal-458, the reflected light at the PBG also played no role at all, as TiO_2 has no absorption in the wavelength of ~458 nm. The results suggested that the more overlap between the PBG of PCs and the absorption edge of TiO_2, the higher the light-harvesting enhancement of TiO_2 coupled with PCs, and therefore the higher the photocatalytic performance of nc-TiO_2.

The light-harvest enhancement of nc-TiO_2 by PCs was further investigated through photodegradation of acetaldehyde under monochromatic light irradiation. The transmission spectrum of the band-pass filter of 380 nm in Fig. 6 shows that the transmittance of the band-pass filter exceeds 85 % in the spectral range of 375–385 nm, which is in accordance with the absorption edge of nc-TiO_2. For SiO_2 opal-333 and SiO_2 opal-458, there was no overlapping between the PBGs and the illumination window. In these cases, the photocatalytic performance under monochromatic irradiation at 380 nm should not be affected by the reflection of PBGs at 333 and 458 nm. Therefore, in the monochromatic light irradiation experiments, SiO_2 opal-333 and SiO_2 opal-458 samples were not used, while the nc-TiO_2/SiO_2 opal-350, nc-TiO_2/SiO_2 opal-380, and nc-TiO_2/SiO_2 opal-400 samples were investigated. The photodegradation experiment results are shown in Fig. 9. The kinetic constants of the first-order photodegradation are listed in Table 2. Similarly, the enhancement factor (EF) is used to evaluate the enhancement of photocatalytic activity. Figure 10 shows the plot of EF versus PBG wavelength under monochromatic light irradiation at 380 nm.

The PBG of SiO_2 opal-380 was centered at 380 nm, completely included in the spectral range of monochromatic light irradiation, and had a strong reflection in the full spectral range. Consequently, the photodegradation rate of acetaldehyde over nc-TiO_2/SiO_2 opal-380 was significantly faster than that on nc-TiO_2/SiO_2-dis, with the EF of 1.5, owing to the enhanced light harvest of nc-TiO_2 by the strong stop-band reflection of PCs and the resultant photon localized in nc-TiO_2. Whereas for the SiO_2 opal-350 and SiO_2 opal-400, only the red edge or blue edge of the PBGs overlapped with the illumination window, and the reflection intensity of SiO_2 opal-350 and SiO_2 opal-400 in the range of irradiation was far weaker than that of SiO_2 opal-380. Therefore, the photocatalytic activity of nc-TiO_2/SiO_2 opal-350 and nc-TiO_2/SiO_2 opal-400 increased by only 10 % in compared with the nc-TiO_2/SiO_2-dis. The PBG-dependent photoactivity of nc-TiO_2 under

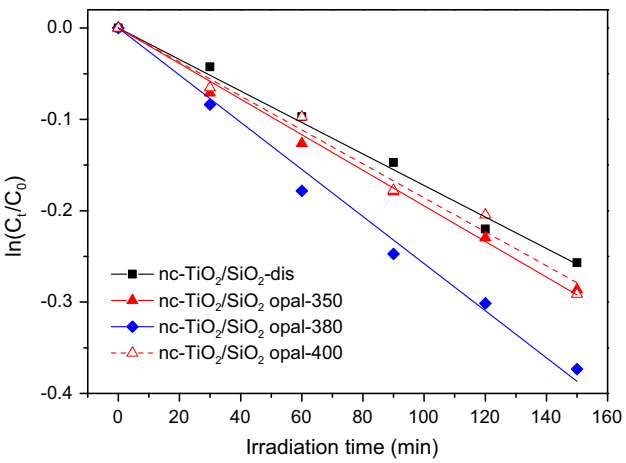

Fig. 9 The first-order photodegradation of acetaldehyde over nc-TiO_2/SiO_2 opal under 380 nm monochromatic light irradiation of 1.2 mW cm^{-2}. The reaction condition was as same as that under white light irradiation: room temperature, 5 cm^{-2} of the photocatalyst film in 872 mL reactor filled with air of 25 % relative water humidity and 200 ppmv gaseous acetaldehyde (Color figure online)

Table 2 Kinetic constants and regression coefficients (R^2) of acetaldehyde degradation under 380 nm monochromatic light irradiation of 1.2 mW cm^{-2}

Sample	Kinetic constant ($\times 10^{-3}$ min^{-1})	R^2
nc-TiO_2/SiO_2-dis	1.72	0.992
nc-TiO_2/SiO_2 opal-350	1.95	0.994
nc-TiO_2/SiO_2 opal-380	2.58	0.989
nc-TiO_2/SiO_2 opal-400	1.86	0.984

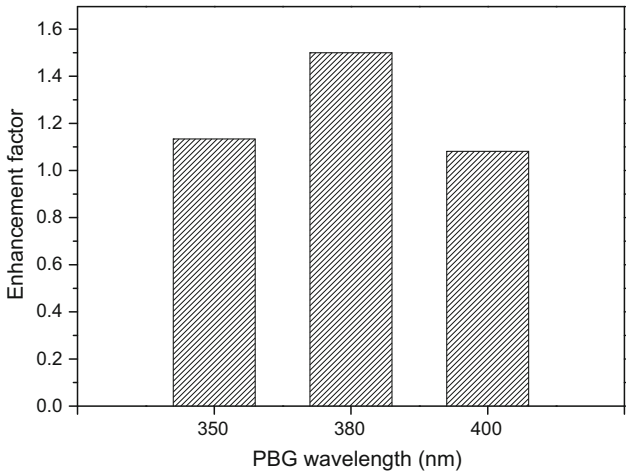

Fig. 10 Enhancement factor for nc-TiO_2/SiO_2 opals under 380 nm of monochromatic light irradiation in comparison to the control of nc-TiO_2/SiO_2-dis

monochromatic light irradiation of 380 nm once again supported the conclusion that the enhanced photoactivity was attributed to the light-harvesting enhancement, which was resulted from the absorption of photons reflected by PCs at PBG and the photon localization in nc-TiO_2.

The reflectance spectra of nc-TiO_2/SiO_2 opal-333, nc-TiO_2/SiO_2 opal-350, nc-TiO_2/SiO_2 opal-380, nc-TiO_2/SiO_2 opal-400, and nc-TiO_2/SiO_2 opal-458 are shown in Fig. 11. Compared with Fig. 6, a drop in the peak intensity at PBG is observed for all PCs when coupled with nc-TiO_2 layer. These drops are owing to the light absorptions during its first pass and second pass (reflection) through the TiO_2 layer. In the case of nc-TiO_2/SiO_2 opal-458 and nc-TiO_2/SiO_2 opal-400, the light absorption of TiO_2 at the PBGs is negligible, so the reflected light plays slight role on enhancing the optical absorption of TiO_2. In the case of nc-TiO_2/SiO_2 opal-380, nc-TiO_2/SiO_2 opal-350, and nc-TiO_2/SiO_2 opal-333, with the PBG changing from 380 to 333 nm, the light absorption of TiO_2 at PCs' PBG becomes higher and higher, and therefore, the drop in reflectance

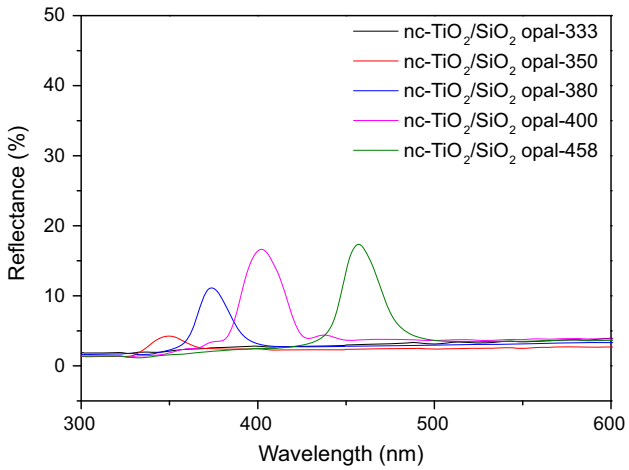

Fig. 11 The UV–Vis reflectance spectra of nc-TiO_2/SiO_2 opal-333, nc-TiO_2/SiO_2 opal-350, nc-TiO_2/SiO_2 opal-380, nc-TiO_2/SiO_2 opal-400, nc-TiO_2/SiO_2 opal-458 (Color figure online)

becomes more significant. Especially for nc-TiO_2/SiO_2 opal-333, the light at the PCs' PBG would be completely absorbed by nc-TiO_2 film before it got to the SiO_2 opal-333, so there is no reflection peak in the spectrum. For nc-TiO_2/SiO_2 opal-350, only a small portion of light will penetrate and then be reflected back into the nc-TiO_2 layer, and therefore, the enhanced effect of nc-TiO_2/SiO_2 opal-350 is also slight. For nc-TiO_2/SiO_2 opal-380, there is considerable part of reflected light localized in TiO_2 and then reabsorbed by TiO_2. Thus, nc-TiO_2/SiO_2 opal-380 shows the highest enhancement factor of the light absorption of TiO_2 and the highest photocatalytic activity.

These results indicated that the photoactivity enhancement by coupling PCs to a photoactive material could be achieved only in the absorption edge of the photoactive material as a consequence of the PBG's reflection of the PCs and its induced photon localization in the photoactive material. The optimum photocatalytic activity of the composite catalyst can be obtained when the PBG of PCs is totally overlapped with the absorption edge of the photoactive material. A 20–30 nm shift of PBG through the change of the SiO_2 particle diameter causes a 80 % drop of the enhancement. In addition, a larger enhancement can be expected when the reflectance intensity at the PBG of the PCs is maximized. This reflectance intensity depends basically on the dielectric contrast [40] and the period number of PCs [41, 42]. So, the PCs can be modified to make better use of the solar energy by increasing refractive index contrast and periodicity-number. These results are of importance to the design of the photonic-crystal-based composite photocatalysts.

Conclusion

We have demonstrated that photoactivity of anatase nc-TiO_2 is remarkably enhanced by coupling it with a SiO_2 opal PCs, and the enhancement factor increases with the increased overlap between the PBG of the SiO_2 opal PCs and EBG of TiO_2. The enhancement is attributed to the light-harvesting improvement of nc-TiO_2 owing to the second absorption of reflected photons and sustained interaction of localized photons with TiO_2. This work provides valuable information for the light-harvesting enhancement in the field of solar energy utilization such as solar cells, environment photocatalysis, and optical communications.

Acknowledgements This research work was supported by the National Nature Science Foundation of China (Grant No. 21376260).

References

1. Pelaez M, Nolan NT, Pillai SC et al (2012) A review on the visible light active titanium dioxide photocatalysts for environmental applications. Appl Catal B-Environ 125:331–349. doi:10.1016/j.apcatb.2012.05.036
2. Cho Y, Choi W, Lee CH, Hyeon T, Lee HI (2001) Visible light-induced degradation of carbon tetrachloride on dye-sensitized TiO_2. Environ Sci Technol 35:966–970. doi:10.1021/es001245e
3. Cheng CW, Karuturi SK, Liu LJ et al (2012) Quantum-dot-sensitized TiO_2 inverse opals for photoelectrochemical hydrogen generation. Small 8:37–42. doi:10.1002/smll.201101660
4. Soejima T, Yagyu H, Ito S (2011) One-pot synthesis and photocatalytic activity of Fe-doped TiO_2 films with anatase–rutile nanojunction prepared by plasma electrolytic oxidation. J Mater Sci 46:5378–5384. doi:10.1007/s10853-011-5476-x
5. Devi LG, Kavitha R (2013) A review on non metal ion doped titania for the photocatalytic degradation of organic pollutants under UV/solar light: role of photogenerated charge carrier dynamics in enhancing the activity. Appl Catal B-Environ 140–141:559–587. doi:10.1007/s10853-011-5476-x
6. Chen QH, Liu HL, Xin YJ, Cheng XW (2014) Coupling immobilized TiO_2 nanobelts and Au nanoparticles for enhanced photocatalytic and photoelectrocatalytic activity and mechanism insights. Chem Eng J 241:145–154. doi:10.1016/j.cej.2013.12.028
7. Hore S, Nitz P, Vetter C, Prahl C, Niggemann M, Kern R (2005) Scattering spherical voids in nanocrystalline TiO_2-enhancement of efficiency in dye-sensitized solar cells. Chem Commun 15:2011–2013. doi:10.1039/b418658n
8. Hall AS, Faryad M, Barber GD et al (2013) Broadband light absorption with multiple surface plasmon polariton waves excited at the interface of a metallic grating and photonic crystal. ACS Nano 7:4995–5007
9. Chen JIL, von Freymann G, Choi SY, Kitaev V, Ozin GA (2006) Amplified photochemistry with slow photons. Adv Mater 18:1915–1919. doi:10.1002/adma.200600588
10. Dinh CT, Yen H, Kleitz K, Do TO (2014) Three-dimensional ordered assembly of thin-shell Au/TiO_2 hollow nanospheres for enhanced visible-light-driven photocatalysis. Angew Chem Int Ed 53:6618–6623. doi:10.1002/anie.201400966
11. Wu M, Liu J, Jin J et al (2014) Probing significant light absorption enhancement of titania inverse opal films for highly exalted photocatalytic degradation of dye pollutants. Appl Catal B-Environ 150–151:411–420. doi:10.1016/j.apcatb.2013.12.037
12. Chen JI, Ozin GA (2009) Heterogeneous photocatalysis with inverse titania opals: probing structural and photonic effects. J Mater Chem 19:2675–2678. doi:10.1039/b900965e
13. Lalitha K, Sadanandam G, Kumari VD, Subrahmanyam M, Sreedhar B, Hebalkar NY (2010) Highly stabilized and finely dispersed Cu_2O/TiO_2: a promising visible sensitive photocatalyst for continuous production of hydrogen from glycerol: water mixtures. J Phys Chem C 114:22181–22189. doi:10.1021/jp107405u
14. Jiao J, Wei Y, Zhao Z et al (2014) Photocatalysts of 3D ordered macroporous TiO_2-supported CeO_2 nanolayers: design, preparation, and their catalytic performances for the reduction of CO_2 with H_2O under simulated solar irradiation. Ind Eng Chem Res 53:17345–17354
15. Zhang X, Liu Y, Lee ST, Yang S, Kang Z (2014) Coupling surface plasmon resonance of gold nanoparticles with slow-photon-effect of TiO_2 photonic crystals for synergistically enhanced photoelectrochemical water splitting. Energy Environ Sci 7:1409–1419. doi:10.1039/c3ee43278e
16. Chen Z, Fang L, Dong W, Zheng F, Shen M, Wang J (2014) Inverse opal structured Ag/TiO_2 plasmonic photocatalyst prepared by pulsed current deposition and its enhanced visible light photocatalytic activity. J Mater Chem A 2:824–832. doi:10.1039/c3ta13985a
17. Xiao JY, Huang QL, Xu J et al (2014) CdS/CdSe co-sensitized solar cells based on a new SnO_2 photoanode with a three-dimensionally interconnected ordered porous structure. J Phys Chem C 118:4007–4015. doi:10.1021/jp411922e
18. Huang Z, Fang L, Dong W, Liu Y, Kang Z (2014) Design and fabrication of carbon quantum dots/TiO_2 photonic crystal complex with enhanced photocatalytic activity. J Nanosci Nanotechnol 14:4156–4163. doi:10.1166/jnn.2014.8276
19. Xu J, Yang B, Wu M, Fu Z, Lv Y, Zhao Y (2010) Novel N–F-codoped TiO_2 inverse opal with a hierarchical meso-/macroporous structure: synthesis, characterization, and photocatalysis. J Phys Chem C 114:15251–15259. doi:10.1021/jp101168y
20. Chen JIL, Loso E, Ebrahim N, Ozin GA (2008) Synergy of slow photon and chemically amplified photochemistry in platinum nanocluster-loaded inverse titania opals. J Am Chem Soc 130:5420–5421. doi:10.1021/ja800288f
21. Sordello F, Minero C (2015) Photocatalytic hydrogen production on Pt-loaded TiO_2 inverse opals. Appl Catal B-Environ 163:452–458. doi:10.1016/j.apcatb.2014.08.028
22. Yuan LF, Yu Z, Li CH et al (2014) PANI-sensitized N-TiO_2 inverse opals with enhanced photoelectrochemical performance and photocatalytic activity. J Electrochem Soc 161:H332–H336. doi:10.1149/2.069405jes
23. Liao G, Chen S, Quan X, Chen H, Zhang Y (2010) Photonic crystal coupled TiO_2/polymer hybrid for efficient photocatalysis under visible light irradiation. Environ Sci Technol 44:3481–3485. doi:10.1021/es903833f
24. Mihi A, Míguez H (2005) Origin of light-harvesting enhancement in colloidal-photonic-crystal-based dye-sensitized solar cells. J Phys Chem B 109:15968–15976
25. Mihi A, Calvo ME, Anta JA, Míguez H (2008) Spectral response of opal-based dye-sensitized solar cells. J Phys Chem C 112:13–17. doi:10.1021/jp7105633
26. Heiniger LP, O'Brien PG, Soheilnia N et al (2013) See-through dye-sensitized solar cells: photonic reflectors for tandem and building integrated photovoltaics. Adv Mater 25:5734–5741. doi:10.1002/adma.201302113

27. Chen SL, Wang AJ, Hu CT, Dai C, Benziger JB (2012) Enhanced photocatalytic performance of nanocrystalline TiO_2 membrane by both slow photons and stop-band reflection of photonic crystals. AIChE J 58:568–572. doi:10.1002/aic.12712
28. Chen SL, Wang AJ, Dai C, Benziger JB, Liu XC (2014) The effect of photonic band gap on the photo-catalytic activity of nc-TiO_2/SnO_2 photonic crystal composite membranes. Chem Eng J 249:48–53. doi:10.1016/j.cej.2014.03.075
29. Chen SL (1998) Preparation of monosize silica spheres and their crystalline stack. Colloids Surf A 142:59–63. doi:10.1016/S0927-7757(98)00276-3
30. Wang AJ, Chen SL, Dong P (2009) Rapid fabrication of a large-area 3D silica colloidal crystal thin film by a room temperature floating self-assembly method. Mater Lett 63:1586–1589. doi:10.1016/j.matlet.2009.04.024
31. Wang AJ, Chen SL, Dong P (2011) Fabrication of colloidal crystal heterostructures by a room temperature floating self-assembly method. Mater Chem Phys 128:6–9. doi:10.1016/j.matchemphys.2011.02.051
32. Ito S, Murakami TN, Comte P et al (2008) Fabrication of thin film dye sensitized solar cells with solar to electric power conversion efficiency over 10 %. Thin Solid Films 516:4613–4619. doi:10.1016/j.tsf.2007.05.090
33. Tamiolakis I, Lykakis IN, Armatas GS (2015) Mesoporous CdS-sensitized TiO_2 nanoparticle assemblies with enhanced photocatalytic properties: selective aerobic oxidation of benzyl alcohols. Catal Today 250:180–186. doi:10.1016/j.cattod.2014.03.047
34. Lin HJ, Yang TS, Hsi CS, Wang MC, Lee KC (2014) Optical and photocatalytic properties of Fe^{3+}-doped TiO_2 thin films prepared by a sol-gel spin coating. Ceram Int 40:10633–10640. doi:10.1016/j.ceramint.2014.03.046
35. Gu ZZ, Fujishima A, Sato O (2002) Fabrication of high-quality opal films with controllable thickness. Chem Mater 14:760–765. doi:10.1021/cm0108435
36. Chen JIL, Gv Freymann, Kitaev V, Ozin GA (2007) Effect of disorder on the optically amplified photocatalytic efficiency of titania inverse opals. J Am Chem Soc 129:1196–1202. doi:10.1021/ja066102s
37. Shang J, Yao W, Zhu Y, Wu N (2004) Structure and photocatalytic performances of glass/SnO_2/TiO_2 interface composite film. Appl Catal A-Gen 257:25–32. doi:10.1016/j.apcata.2003.07.001
38. Lozano G, Colodrero S, Caulier O, Calvo ME, Hn Míguez (2010) Theoretical analysis of the performance of one-dimensional photonic crystal-based dye-sensitized solar cells. J Phys Chem C 114:3681–3687. doi:10.1021/jp9096315
39. Lu Y, Yu H, Chen S, Quan X, Zhao H (2012) Integrating plasmonic nanoparticles with TiO_2 photonic crystal for enhancement of visible-light-driven photocatalysis. Environ Sci Technol 46:1724–1730. doi:10.1021/es202669y
40. Kubo S, Gu ZZ, Takahashi K, Ohko Y, Sato O, Fujishima A (2002) Control of the optical band structure of liquid crystal infiltrated inverse opal by a photoinduced nematic-isotropic phase transition. J Am Chem Soc 124:10950–10951. doi:10.1021/ja026482r
41. Bertone JF, Jiang P, Hwang KS, Mittleman DM, Colvin VL (1999) Thickness dependence of the optical properties of ordered silica-air and air-polymer photonic crystals. Phys Rev Lett 83:300. doi:10.1103/PhysRevLett.83.300
42. Liu JT, Wang TB, Li XJ, Liu NH (2014) Enhanced absorption of monolayer MoS_2 with resonant back reflector. J Appl Phys 115:193511. doi:10.1063/1.4878700